A major purpose of the Technical Information Center is to provide the broadest dissemination possible of information contained in DOE's Research and Development Reports to business, industry, the academic community, and federal, state and local governments.

Although a small portion of this report is not reproducible, it is being made available to expedite the availability of information on the research discussed herein.

LA-UR--86-3855

DE87 002906

TITLE THE KURAMOTO-SIVASHINSKY EQUATION: SPATIO-TEMPORAL CHAOS AND INTERMITTENCIES FOR A DYNAMICAL SYSTEM

AUTHOR(S) BASIL NICOLAENKO

CENTER FOR NONLINEAR STUDIES

SUBMITTED TO PROCEEDINGS OF CONFERENCE ON PHYSICO-CHEMICAL HYDRODYNAMIC INSTABILITIES, PLENUM PRESS HELD IN LA RABIDA (HUELVA) SPAIN, JULY 11-16, 1986

DISCLAIMER

Los Alamos National Laboratory
Los Alamos, New Mexico 87545

THE KURAMOTO-SIVASHINSKY EQUATION: SPATIO-TEMPORAL CHAOS AND INTERMITTENCIES FOR A DYNAMICAL SYSTEM

Basil Nicolaenko
Center for Nonlinear Studies and Theoretical Division
Los Alamos National Laboratory
Los Alamos, New Mexico 87545, U.S.A.

ABSTRACT

We survey some recent results on the finite-dimensional behavior of the Kuramoto-Sivashinsky equation. We outline how it is rigorously equivalent to a finite dimensional dynamical system on a finite "inertial" manifold; a geometric approach to the construction of such a manifold is given. We give some examples of computational simulations supporting the evidence for a low-dimensional vector field which rules the bifurcations of the inertial manifold.

I. INTRODUCTION

During the last decade we have seen a number of major developments which show that the long-time behavior of solutions of a very large class of partial differential equations (PDEs) possess a striking resemblance to the behavior of solution of finite dimensional dynamical systems, or ordinary differential equations (ODEs). The first of these advances was the discovery (by a number of researchers) that a dissipative PDE has a compact, maximal attractor X with finite Hausdorff and fractal dimensions. More recently [6, 12-15] it was shown that some of these PDEs possess a finite dimensional inertial manifold, i.e., an invariant manifold that contains the attractor X. For the later equation, the connection with ODEs is no longer a mere resemblance, instead it has become a striking reality! The reason for this is that where one restricts the PDE to the inertial manifold one obtains an ODE, which we call an inertial form for the given PDE. Since an inertial manifold contains the universal attractor, this means that the long-time behavior of solutions of a PDE with an inertial manifold is completely determined by the inertial form.

There is, indeed, a class of phenomena of incipient turbulence which can be modeled by scalar field PDEs undistinguishable in practice from dynamical systems: weak turbulence on interfaces between complex flows, upon which appear well localized patterns and structures. Such are quasiplanar flame fronts; thin viscous fluid films flowing over inclined planes; and even, under some conditions, dendritic phase change fronts in binary alloy mixtures [30-31, 38, 40-42]. In such physical contexts, the onset of destabilization of the simplest laminar regime is heralded by the cohesive organization of cells and patterns (often hexagonal) on the moving and buckling front or interface.

Many such interfaces with localized turbulence, including flames, can be modeled by the simple Kuramoto-Sivashinsky (K-S) PDE [33-36, 38]. This equation accurately accounts for the thermo-diffusive and convective mechanics of flow-field coupling across an interface before turbulence breaks away from the interface and reaches deeply into the fluid.

In one space dimension, the K-S equation modeling a small perturbation u(x,t) of a metastable planar front or interface is

$$\begin{aligned} u_t + \nu u_{xxxx} + u_{xx} + \frac{1}{2}(u_x)^2 = 0 \ , \ (x,t) \epsilon R^1 \times R_+ , \\ u(x,0) = u_o(x) \ , \ u(x+L) = u(x,t) \end{aligned} \tag{1.1}$$

Here the subscripts indicate partial differentiation, ν is a positive fourth-order viscosity and u_o is L-periodic; L being the size of a typical pattern scale. The natural bifurcation parameter is the renormalized dimensionless parameter $\tilde{L} = L/(2\pi\sqrt{\nu})$. $[\tilde{L}]$ is also the number of linearly unstable Fourier modes, where the symbol $[\ ]$ designates the integer part of a real number.

In a previous work our computer simulations of the K-S equation [28] demonstrated an uncanny, low-dimensional behavior for the values of the bifurcation parameter up to $\tilde{L}$ = 3.67 (L = 23.1). A low dimensional structure does also underline an example of onset of chaos at $\tilde{L}$ = 5.42 (L = 34.05). In general, the attracting solution manifolds undergo a complex bifurcation sequence including multimodel fixed points, invariant tori, traveling wave trains and homoclinic orbits. Moreover, amidst lengthy and complex chaotic time series, puzzling intermittencies do occur at random: these are protracted oscillations in a small neighborhood of some metastable state. We conjectured in [28] that such a behavior shadows a perturbed homoclinic orbit and betrays a hidden underlying low-dimensional dynamical system.

The long time behavior of such smooth dissipative differential systems is characterized by the presence of an universal attractor X toward which all trajectories converge. The structure of X may be very complicated even in the case of simple ordinary differential equations: X may be a fractal on parafractal set. In the case of dissipative partial differential equations, although the phase space (i.e. the function space) is an infinite dimensional space, X has finite fractal dimension (see [2-5] [41-42]). However, the already possibly complex nature of X is in this case further complicated by the infinite number of degrees of freedom of the ambient space. In the case the dissipative system admits an inertial manifold the attractor is dynamically embedded in a finite dimensional manifold and thus becomes the attractor of a dynamical system with a finite number of degrees of freedom.

Since [28], it has indeed been demonstrated that the K-S equations are rigorously equivalent to a finite-dimensional dynamical system. The approach (introduced in [12-15]) consists in constructing a finite dimensional Lifschitz manifold $\sum$ (called inertial) in the phase space of the PDE such that:

(i) $\sum$ is invariant and has compact support; that is if $(S(t,\cdot))_{t\geq 0}$ is the nonlinear semigroup associated with the initial value problem for the equations, then $S(t,\sum)$ is contained in $\sum$ for all $t \geq 0$.

(ii) All solutions converge exponentially to $\sum$. In particular, the universal attractor, X, is included in $\sum$ and the dissipative system reduces on $\sum$ to a finite system (called an inertial ODE).

(iii) asymptotic completeness holds: for every initial value for the full K-S equation, there exists some initial point on the inertial manifold $\sum$ decreases exponentially to zero [6,

The last point does fully establish the equivalence between the PDE and the inertial ODE on $\sum$. Concretely, given a chaotic trajectory for the exact PDE, we can find a finite dimensional chaotic trajectory for the inertial ODE, such that the two trajectories converge exponentially.

The existence of such an inertial manifold has been demonstrated [6, 14, 15, 37] for the K-S equation with Neumann boundary conditions. In similar results hold for a PDE model of 2-D weak turbulence in Kolmogorov shear flows [8].

Hence, weak turbulence on interfaces modelled by the K-S equation is strictly equivalent to chaos for a finite inertial dynamical system. Still, weak spatio-temporal turbulence involves complex mechanisms within the bifurcations of the inertial manifold. To unravel these, we must obtain a clear picture of those few nonlinear states (spatial structures) which form a reduced nonlinear coordinates basis for the manifold. A nonlinear representation of the inertial manifold must be constructed, based on reduced coordinates patches, with the goal of establishing reduced, low-dimensional, inertial normal forms for the inertial ODEs, valid for some range of the bifurcation parameter. These inertial normal forms control the global vector field bifurcations into weak turbulence and ultimately account for the universality of transition to chaos in infinite dimensional systems.

In this conference presentation, we propose to give a partial survey of the questions raised above, in the context of the K-S equation. Rather than another catalogue of bifurcations, we establish that successive transitions to chaos and intermittent relaminarizations are ruled by the stable and unstable manifolds of a small number of nonlinear states. This reduced representative sample changes along with the bifurcation parameter; its dimensionality is much smaller than the rough estimates for the dimension of the inertial manifold obtained in [6, 14-15]. In part III, we evidence such low dimensional canonical vector field bifurcations for regimes within $23.1 \leq L \leq 34.05$ ($3.67 \leq \tilde{L} \leq 5.42$, where $[\tilde{L}]$ is the number of unstable modes); for such regimes, the fractal dimension of chaos does not exceed 5. We have systematically searched for classical dynamical systems bifurcations and for multiple basins of attractions for the K-S model. We used a general PDE solver code developed by J. M. Hyman at LANL [29, 30]. The interactions of multiple basins through their fractalized boundaries have been evidenced. Intermittencies in turbulent time series are one of the key mechanisms in bridging the gap between PDEs and dynamical systems. They enable us to track the unstable manifolds of key hyperbolic points. These intermittencies are random time windows where dynamics remain highly oscillatory yet are confined in a relatively small neighborhood of some metastable point or circle. Such critical states are the natural candidates for local nonlinear coordinates of the inertial manifold.

In part IV, we survey an intrinsic geometric construction of inertial manifolds, inspired by the exponentially fast lock-up of dynamical trajectories onto such manifolds. This surveys joint work with P. Constantine, C. Foias and R. Temam [6]

II. OVERVIEW OF COMPUTATIONAL SIMULATIONS AND THEORETICAL RESULTS

We have normalized the K-S equation to an interval of length 2π; set the damping parameter to the original value derived by Sivashinsky, $\nu = 4$, and introduced the bifurcation parameter $\alpha = 4\tilde{L}^2 = L^2/4\pi^2$. The equation can now be written as

$$\begin{gathered} u_t + 4u_{xxxx} + \alpha[u_{xx} + \frac{1}{2}(u_x)^2] = 0 \ , \ 0 \le x \le 2\pi, \\ u(x+2\pi,t) = u(x,t) \ , \ u(x,0) = u_o(x) \end{gathered} \tag{2.1}$$

This equation is equivalent to Eq. (1.1) with a different time scaling.

The mean value of the solution to Eq. (2.1)

$$m(t) = \frac{1}{2\pi}\int_o^{2\pi} u(x,t)dx \tag{2.2}$$

satisfies the drift equation

$$\dot{m}(t) = \frac{-\alpha}{4\pi}\int_o^{2\pi}(u_x)^2 dx. \tag{2.3}$$

To normalize this drift to zero, we numerically solved the equation for

$$v(x,t) = u(x,t) - m(t). \tag{2.4}$$

That is, the drift-free K-S equation is

$$v_t + 4v_{xxxx} + \alpha[v_{xx} + \frac{1}{2}(v_x)^2] + \dot{m}(t) = 0. \tag{2.5}$$

we have scanned the domain $54 \le \alpha \le 320$, i.e., $3.67 < r \le 8.95, 25.8 < L < 56.2$. Many previous investigations have solved Eq. (1.1) on an interval [0,L], with viscosity $\nu = 1$ [31]. Our rescaled time t in (2.1) and the usual unnormalized time t_{Phys} are related through:

$$t_{Phys} = 4\tilde{L}^4 t = \alpha^2 t/4; \tag{2.6}$$

the rescaling grows quadratically in α. The bifurcations diagrams (Fig. 1, 2, 3) were obtained by scanning in α and varying initial data.

In our computer experiments, we found that high precision was necessary because of the extreme sensitivity of the simulations to numerical accuracy. Nonconverged numerical solutions of Eqs. (1.1) and (2.1) can occur in regimes we are interested in if the time integration errors are greater than 10^{-6} per unit time-step. In fact, small effects of the order of 10^{-6} in the energy for some sensitive Fourier modes critically impact on the nonlinear dynamics. To alleviate this, we use in our calculations high-precision, pseudospectral approximation to the spatial derivatives [9, 10] and a variable time-step, variable-order integration method in time to keep the solution errors between 10^{-8} and 10^{-10} per unit

time [29, 30]. The PDE solver was an all purpose code developed by J. M. Hyman at LANL [29, 30].

A typical example of the extreme numerical sensitivity of the numerical solutions to the K-S equation is the disappearance of homoclinic orbits if the precision is too low. The hyperbolic fixed points degenerate into stable fixed points with a numerically artificial basin of attraction the size of the error control. Because of the artificially stable fixed point, our numerical results of the K-S equation differ from some of the previously published simulations that relied on second-order schemes with only modest control over time integration errors.

We systematically tracked the domains of stability of each attractor with respect to the bifurcation parameter by varying α and reinitializing v(x,o) to the final solution from the previous run with a different α. Many problems were recalculated several times with different grid resolutions and time truncation error criteria to ensure that the numerical solutions were converged within an acceptable accuracy.

A remarkable feature of the K-S equations is the alternating sequence of intervals in α containing laminar behavior (some fixed point is ultimately attracting) with intervals of persistent oscillatory and/or chaotic behavior. Let $I_j = [\alpha_j, \alpha_{j+1}]$ be the j^{th} interval. Then $I_o = [0, \alpha_1]$, where at α_1 comes the first Hopf bifurcation; a classical pitchfork steady-state bifurcation occurs at $\alpha = 4 < \alpha_1$. For j even, I_j is characterized by the ultimate decay to a globally attracting fixed point $\tilde{u}_q(x), q = (j/2)+1, j \geq 2$. These fixed points have most of their energy concentrated in a cos qx mode. The higher harmonics appear with exponentially decreasing energy and the fixed point has a lacunary Fourier expansion:

$$\begin{aligned}\tilde{u}_q(x) =& a_{1q}cosqx + \epsilon a_{2q}cos2qx \\ &+ \epsilon^2 a_{3q}cos3qx + \cdots + \epsilon^{n-1}a_{nq}cosnqx + \cdots,\end{aligned} \tag{2.7}$$

where $q = j/2 + 1$. Numerically, we have found that a_{1q} is O(1) and $\epsilon \cong 10^{-1}$. We call these sinks associated with I_j, j even, cellular states. When the Fourier expansion (2.7) of a cellular state is dominated by cos qx as we call it a q-modal cellular state.

These relaminarization intervals I_j, j even, are consistent with experiments at small and moderate Reynolds numbers [40]. Moreover, as j and α increase, the ultimate decay follows long periods of transient chaos. Transient chaos is observed in the K-S equations beginning in the interval I_4, provided enough modes are excited in the initial data. Moreover, as α increases, the mean lifetime of transient chaos increases exponentially in $\tilde{L}$: this growth makes transient chaotic intervals undistinguishable in practice from chaotic intervals in the strongly chaotic regimes (say, when the fractal dimension of the universal attractor, X, for the flow is large, $dim_F(X) \geq 10$).

When j is odd, the intervals I_j have persistent oscillatory and/or chaotic behavior. For moderate values of α (say, up to I_7), the quasiperiodic and/or chaotic behavior reflects a competition between the previous $(j+1)/2$ cellular state, dominated by the $cos((j+1/2)x)$ mode, and the $(j+3)/2$ cellular state, dominated by $cos((j+3/2)x)$. This competition creates a complex interplay between temporal chaos and spatial coherence. In some sense, the (low-dimensional) temporal chaos corresponds to adjustment from one (low-dimensional) space pattern to the next one. Unfortunately, this simple picture is not borne by our computations at strongly chaotic regimes ($dim_F(X) > 6$) where a zoo of strange hyperbolic fixed points appear in intermittencies. Their strangeness resides in that they are not cellular in the sense of (2.7) and possess a broad energy spectrum band covering all the unstable modes up to $[\tilde{L}]$.

Finally, the best current estimate [15] on the dimension of $\sum$, the inertial manifold for Eq. (2.1) is:

$$dim(\sum) \leq c\alpha^{1.75} , \tag{2.8}$$

which is still too large when compared to the upper estimate of the fractal dimension of the universal attractor X obtained in [36]:

$$d_f(X) \leq c\alpha^{0.75} . \tag{2.9}$$

The severe numerical sensitivity of the K-S equation demonstrates that the dynamics of the inertial ODE and the bifurcations of the inertial manifold are very sensitive to the accuracy of numerical algorithms. Conventional PDE algorithms do not carry over.

III. LOW DIMENSIONAL CHAOS FOR THE KURAMOTO-SIVASHINSKY EQUATION

In this section we describe the behavior of the solutions to the K-S equation for parameter values in the intervals $I_4, I_5, I_6, 54 < \alpha \leq 117.5$, that is $3.67 < \tilde{L} \leq 5.42, 23.1 < L \leq 34.05$. The windows I_1 (oscillatory, $17.3 \leq \alpha \leq 22.5$) I_2 (2-cell state globally attracting, $22.5 < \alpha < 43$) and I_3 (quasiperiodicity, $43 \leq \alpha < 54$) were investigated in [28]; results are summarized in Fig. 1 and Fig. 2. Our preliminary catalogue for the intermediate values of α, $54 \leq \alpha \leq 117.5$, is presented in Fig. 3. It contains a sequence of "laminar" intervals and intervals with complex oscillatory behavior:

I_4	=	$54 < \alpha < 67.5$:	a 3-cellular state global attractor
I_5	=	$67.5 < \alpha < 93$:	complex oscillatory behavior
I_6	=	$93 < \alpha < 117.5$:	a 4-cellular state global attractor
I_7	=	$117.5 < \alpha < 146.5$	chaos

Within these intervals, we evidence canonical vector field bifurcations leading to quasi-periodic motion and chaos, and systematically explore multiple basins of attraction, in a low-dimensional situation. The mechanisms which we pin down are truly generic for both onset of chaos and relaminarization crises in regimes of "strong" chaos (see part IV), and more representative than the bifurcations in $I_1 - I_3$ studied in [28]. The classical homoclinic loop bifurcations from a saddle point observed around $\alpha \sim 22.5$ and $\alpha \sim 43$ do not reoccur; repeated onsets of oscillatory, and/or chaotic regimes are in fact triggered by perturbed homoclinic loops bursting from spiral hyperbolic points. T_1 tori (invariant circles) are usually metastable. Strange fixed points are the rule rather than the exception, spanning the range from $\alpha = 49.5$ through α=93. A travelling beating wave obsreved in Fig. 1b from α=49.5 to α=54 is a true harbinger of such a strange (two-humped) fixed point. Also, there is a wealth of reverse bifurcation, and attractors which alternatively destabilize and restabilize again at some larger α! Last, the crisis of chaos observed at α=93 is likely triggered by the two-humped strange fixed point sitting on the basin boundary of the chaotic attractor and shadowing the turbulent time series through multiple intermittencies. Such low-dimensional mechanisms pervade the strongly chaotic regimes of part IV.

In the discussion below, the "energy" is the integral of $(u_x)^2$ and the "energy in mode k" is the modulus of the k^{th} Fourier coefficient.

The trimodal cellular state $\tilde{u}_3(\alpha)$ is a global attractor in I_4 until it bifurcates at α=67.5. The bifurcation is neither of Hopf type, nor through a classical homoclinic loop. This is explored in Figs. 4-7, where $u_o = \tilde{u}_3(67.5) = 2.95cos3x + 0.44cos6x + \cdots$. Figure 4 heralds two regimes: at roughly periodic intervals the orbit bursts away on the unstable manifold of $\tilde{u}_3$ and puffs into a spiked intermittency at a much lower energy level; then it spirals back around the hyperbolic point $\tilde{u}_3$. Figure 5 confirms that the energy in the first mode is low

during the small oscillations around the spiral hyperbolic point $\tilde{u}_3$; the bursts have a much higher level in the first mode. Small amounts of energy trigger the bursts around the loop. The energy in the third mode, Fig. 6, is the mirror image of Fig. 5. It oscillates in a small neighborhood of 2.9, before bursting away from $\tilde{u}_3$ into sharp spikes at much lower levels. The energy in mode 6 (Fig. 7) is substantial in the vicinity of $\tilde{u}_3$, at a level of 0.4. It clearly shows two different scales in the dynamics of the orbit next to $\tilde{u}_3$; first very high frequency, small amplitude oscillations around $\tilde{u}_3$, followed by slower spiraling around the trimodal point. This bifurcation has many of the characteristics of a perturbed Shilnikov homoclinic loop [25]. This is a homoclinic loop associated with a spiral hyperbolic point and persists until α=72.

The Shilnikov loop is quickly deformed into a homoclinic tangle, as evidenced in Figs. 8-10 (α=68, initial conditions continued from α=67.5). The duration of the chaotic excursions is now comparable to the transit times in the vicinity of $\tilde{u}_3$, any semblance of periodicity is lost and spiked bursts occur at random times (Fig. 8). The energy in mode one (Fig. 9) demonstrates that the high frequency, small oscillations around $\tilde{u}_3$ prevail upon the spiraling time-scale dynamics; a computer movie "zoom" onto such time intervals reveals transient dynamics hardly distinguishable from those on a metastable circle (Torus T_1). Energy in mode 3 (Fig. 10) confirms the picture of an homoclinic tangle between the stable and unstable manifolds of the spiral hyperbolic point $\tilde{u}_3$, with chaotic time series interrupted by random intermittencies around $\tilde{u}_3$. The above generic picture will permeate the onset of chaos at α=117.5.

At α=72, a strange fixed point $u^*(\alpha)$ suddenly becomes a global attractor. It is not related to any cellular state; its Fourier expansion is rather flat, with energy present in all first six modes ($\tilde{L} = 4.24$). u^* has a typical profile with two humps, a large one and a small one (Fig. 11). An entirely similar two-humped structure has been observed as a traveling and beating wave, from α=49.5 to α=54; the strange fixed point $u^*(\alpha)$ has indeed undergone a reverse bifurcation back to stability! It persists as a global sink, until it undergoes some kind of Hopf bifurcation at α=83.75. As the contour levels show in Fig. 12 (α=84.25, initial data by continuation), the rapid oscillations are strictly localized in space, on the top of the higher hump. Such a spatio-temporal localization is a forerunner of spatially concentrated zones of turbulence. This peculiar example of spatial complexity does not seem to be ruled by a standard Hopf mechanism. At α=86, the localized oscillating pattern bifurcates into a travelling beating wave. The contour levels plot (Fig. 13, α=87, initial data by continuation) manifest fast oscillations still localized on the higher hump. At α=89, the picture reverts to chaotic behavior, as if the "horseshoe" attractor observed

from $68 \leq \alpha < 72$ had undergone a basin boundary crisis. The interval I_5 ends at α=93, where the 4-modal cellular state

$$\tilde{u}_4 = 2.94cos4x + 0.28cos8x + \cdots \tag{3.1}$$

mutates into a global sink. The apparent crisis of chaos at α=93 is further complicated by the fact $\tilde{u}_4$ has a limited, albeit small basin of attraction for $90.5 < \alpha \leq 93$. This suggests basin boundary crisis [19-24]. Chaotic time series both prior to and at the crisis exhibit multiple intermittencies around some hyperbolic point, which is obligatory non cellular (since $\tilde{u}_4$ is a local sink). This is illustrated at α=91, with initial data $u_o = \sum_{j=1}^{4}(cosjx+sinjx)$, Figs. 14-17. In Fig. 14, energy in mode one goes through two broad intermittencies; these are characterized by small amplitude, high frequency oscillations at an average level of 4. Within the intermittent windows, energy in mode 2 (Fig. 15), at an average level of 2.5, is comparable to mode 1. The (average) Fourier energy spectrum at the intermittencies is significantly comparable to that of the strange point $u^*(\alpha)$. Movies unmistakedly betray the two-humped structure. Energy in mode 3 (Fig. 16) confirms high frequency, small scale oscillations whenever the orbit wanders close to the stable manifold of u^*; as if the boundary of the basin for the chaotic attractor were vested with multiple fingers close to that stable manifold. Energy in mode 4 (Fig. 17) confirms that u* sits on the boundary delineating the basins of $\tilde{u}_4$ and is responsible for this basin boundary crisis [19-24].

The interval I_4 of global stability for $\tilde{u}_4$ ends at α=117.5. In [28] we suspected some homoclinic skeleton to underline the onset of chaos at α=117.5. We can now give a much more precise microscopy of this bifurcation. At α=117.5, we took for initial data

$$\tilde{u}_4 + 0.1sinx = 0.1sinx + 2.995cos4x + 0.43cos8x + \cdots. \tag{3.2}$$

The time series in Figs. 18-20 are remarkably akin to, albeit more chaotic than those for the perturbed Shilnikov loop in Figs. 8-11; just replace $\tilde{u}_3$ by $\tilde{u}_4$. The energy (Fig. 18) undergoes very high frequency oscillations within intermittencies close to the quadrimodal state, before exploding into chaos with an higher average energy. The energy in mode 2 (Fig. 19) dips at very small levels in the vicinity of $\tilde{u}_4$. The energy in mode 4 (Fig. 20) clearly shows the orbit nearly locking onto some metastable torus, around 2.9 before bursting into homoclinic tangles. For the energy in mode 8 (Fig. 21), the intermittencies center at 0.4; this confirms the picture of a perturbed Shilnikov tangle around $\tilde{u}_4$, as a mechanism for onset of chaos. As computed by Manneville [35], the Lyapunov dimension of chaos is slightly larger than 5 in this case.

The bifurcations of the K-S equation, unravelled in this part, occur on low-dimensional inertial manifolds. Multiple forward and reverse bifurcations of several fixed points are

entangled in a web of Tori, together with "strange" hyperbolic points. For these regimes, we conjecture that it may be possible to construct a simple reduced normal form for the ODEs on the inertial manifold using the unstable manifolds of $\tilde{u}_3(\alpha), (\tilde{u}_4(\alpha)$ and the two-humped "strange" fixed point $u^*(\alpha)$.

IV. A GEOMETRIC CONSTRUCTION OF THE INERTIAL MANIFOLDS

The K-S equations possess inertial manifolds $\sum$. These are positively invariant regular objects toward which all solutions tend at (at least) a uniform exponential rate. Let H be the Hilbert phase space (usually a Sobolev space) and let $S(t)u_0)$ denote the trajectory (solution of the system) starting at $t = 0$ from u_0. By an inertial manifold for $S(t)$ we mean a set $\sum$ satisfying

$$\overline{\sum} \text{ is a finite dimensional Lipschitz manifold} \tag{4.1}$$

$$S(t)\overline{\sum} \subset \overline{\sum} \text{ for } t \geq 0 \tag{4.2}$$

$$\text{There exists a constant k such that for every } u_0 \epsilon H \text{ , there exists } t_0 \geq 0 \tag{4.3}$$

(uniformly for u_0 in bounded sets) such that, for $t \geq t_0$

$$dist(S(t)u_0 \ , \ \overline{\sum})$$

$$\leq dist(S(t_0)u_0, \overline{\sum})exp(-Kt)$$

We shall present here a geometric method of constructing $\sum$ for a class of dissipative systems large enough to contain the one dimensional Kuramoto-Sivashinski and one and two dimensional parabolic reaction diffusion equations. Full details will be found in a forthcoming paper by P. Constantire, C. Foias, R. Temam and B. Nichols [6]. The K-S equation can be restated abstractly as:

$$\frac{du}{dt} + N(u) = 0 \text{ with} \tag{4.4}$$

$$N(u) = Au + R(u) \tag{4.5}$$

where A is a positive selfadjoint operator and $R(u)$ is a lower order nonlinear nonhomogeneous term. We denote by $(\lambda_j)_j$ the increasing sequence of distinct eigenvalue of A and J_y (λ_j) the nondecreasing sequence of eigenvalues counted with their multiplicities. The linearized around $u(t)$ of $N(u)$, will be denoted by $A(t)$

$$L(t)v = \frac{\partial R}{\partial u}(u(t))v \ , \ A(t) = A + L(t) \tag{4.6}$$

The key idea is to use the transport properties of finite dimensional contact elements. By a finite dimensional contact element we mean a pair (u_0, P_0) with $u_o \in H$ and P_0 a

finite dimensional projector (orthogonal projection operator) in H. One regards P_0 as the projector on the tangent space at u_0 to an infinitesimal surface passing through u_0. The transport under $S(t)$ of this surface induces the transport of (u_0, P_0) according to

$$u(t) = S(t)u_0 \tag{4.7}$$

$$\frac{d}{dt}P(t) + (I - P(t))A(t)P(t) + P(t)A(t)^*(I - P(t)) = 0 \tag{4.8}$$

$$P(0) = P_0 \tag{4.9}$$

where $A(t)$ is the linearized (0 6) and $A(t)^*$ is the adjoint in H. For any N dimensional contact element (u, P) we introduce the quantities

$$\Lambda(u) = Max\{(Ag, g) || g| = 1\ ,\ Pg = g\ ,\ g \in D(A)\} \tag{4.10}$$

$$\lambda(u) = Min\{(Ag, g) || g| = 1\ ,\ Pg = 0\ ,\ g \in D(A)\} \tag{4.11}$$

where $(,)$ and $||$ denote the scalar product and the norm in H; $D(A)$ is the domain of A. It follows from the minimax and mimimin theorem that $\Lambda(u) \geq \lambda_N$, $\lambda(u) \leq \lambda_{N+1}$. These two quantities measure the position of the linear space $ker(I - P)$ relative to the fixed orthonormal system of coordinates formed with the eigenvectors (w_j) of $(Aw_j = \lambda_j w_j)$. We assume that $L(t)$ satisfy bounds of the type

$$|L(t)v|^2 \leq K_2|v|^2 + K_2|Av^{1/4}|^2 + K_3|A_v^{1/2}|^2 \tag{4.12}$$

$$|L(t)^*v|^2 \leq K_1|v|^2 + K_2|Av^{1/4}|^2 + K_3|A_v^{1/2}|^2 \tag{4.13}$$

reflecting the fact that $R(u)$ is assumed to be of lower order (half the number of derivatives at most) than A. We derive under these assumptions differential inequalities for the transported quantities $\lambda(t) = \lambda(P(t))$ $\Lambda = \Lambda(P(t))$. If the linear diffusion operator A has gaps in the spectrum which are large with respect to constant K_1, K_2, K_3 more precisely if

$$(\Lambda_{m+1} - \Lambda_m)^2 > K_1 + K_2\left(\frac{\Lambda_m + \Lambda_{m+1}}{2}\right)^{1/2} + K_3\frac{\Lambda_m + \Lambda_{m+1}}{2} \tag{4.14}$$

for some m, then we can deduce the powerful spectral blocking proposition:

Theorem 4.1 (Spectral blocking property).

Let $\lambda(t) = \lambda(P(t))$ $\Lambda(t) = \Lambda(P(t))$ be defined in (4.10), (4.11) for $P(t)$ solving (4.7)-(4.9), then

$$\text{if for some } t_0 \geq 0\ \Lambda(t_0) < \frac{\Lambda_m + \Lambda_{m+1}}{2} \tag{a}$$

for some m satisfying (4.14) then $\Lambda(t) < \frac{\Lambda_m + \Lambda_{m+1}}{2}$ for all $t \geq t_0$,

$$\text{if for some } t_0 \geq 0\ ,\ \lambda(t_0) > \frac{\Lambda_m + \Lambda_{m+1}}{2} \tag{b}$$

for some (possibly different) m satisfying (4.14) then $\lambda(t) > \frac{\Lambda_m+\Lambda_{m+1}}{2}$ for all $t \geq t_0$. Thus $\lambda(t)(resp A(t))$ cannot cross large gaps in the spectrum of A from the right (resp left).

We note here that although a condition of the type $\lambda(t_0) > \frac{\Lambda_m+\Lambda_{m+1}}{2}$ can be realized only if the dimension N of $P(t_0)$ is large enough ($\lambda_{N+1} > \frac{\Lambda_m+\Lambda_{m+1}}{2}$) conditions of the type $A(t_0) < \frac{\Lambda_m+\Lambda_{m+1}}{2}$ do not impose restrictions on the dimension of $P(t_0)$ provided the set of m's for which (4.14) is valid is not founded. In particular the blocking of $A(t)$ in the $N = 1$ case has important consequences. Let us denote by P_m the spectral projector of A on the span of $w_1, \cdots, w_m$. Let us consider the cone in H

$$c = \{\omega \epsilon H || (I - P_n)\omega| \leq \frac{1}{3}|P_n\omega)\} \tag{4.15}$$

We prove the strong squeezing properties.

Theorem 4.2 Let n be large enough. Let $\omega(t)$ be a solution of

$$\begin{aligned} \frac{d\omega}{dt} + A(t)\omega = 0 \ , \\ \omega(0) = \omega_0 \ , \end{aligned} \tag{4.16}$$

the linearized equation around $S(t)u_0 = u(t)$. If for some $t_0 \geq 0$ $\omega(t_0)$ belongs to C, then for all $t \geq 0$ $\omega(t)$ belongs to C. Moreover, the following alternative holds:

$$|\omega(t)| \leq |\omega(0)| exp(-Kt) \text{ for all } t \geq 0 \tag{a}$$

or there exists a finite

$$t_0 > 0 \text{ such that the irregularity in (a) holds for } t \leq t_0 \text{ and for } t \geq t_0 \omega(t) \text{ belongs to C.} \tag{b}$$

The precise condition on the size of n is given in [8], but essentially the requirement is that $\lambda_n > 5(\Lambda_m + \Lambda_{m+1})$ for some n satisfying the gap condition (4.14) Theorem 4.2 is a direct consequence of Theorem 4.1 for $N = 1$. Using a slight modification of Theorem 4.1. We obtain, also,

Theorem 4.3 (Strong squeezing property) let n be large enough (same conditions as in Theorem 4.2). Let $\omega(t) = S(t)u_0 - S(t)u$ be the difference of two solutions. Then the conclusions of Theorem 4.2 hold for $\omega(t)$. The strong squeezing property was established for the Kuramoto-Sivashinski equation in [15]. The consequences of this property regarding the universal attractor are studied further. We prove

Theorem 4.4. If n is large enough to insure the validity of Theorem 4.3 then the projector P_n is injective when restricted to the universal attractor X and its inverse is Lipschitz. More precisely

$$|(1 - P_n)(x - y)| \leq \frac{1}{3}|\Gamma_n(x - y)|$$

for every x,y in X.

Theorem (4.4) follows easily from Theorem 4.3 but is an important fact. It was known that because X has finite fractal dimension, there are many projectors that are injective on X; however, P_n is an important explicit one.

Denoting $C_{n,X} = x\epsilon X\{u \in H||(1-P_n)(u-X)| \leq \frac{1}{3}|P_n(u-x)|\}$ we deduce from Theorem 4.3 that $S(t)C_{n,X} \subset C_{n,X}$ if n is large enough, that $X \subset C_{n,X}$ (Theorem 4.4) and that as long as a solution $S(t)u_0$ remains in the complement of $C_{n,X}$, its distance to X decreases exponentially. Finally, we conclude by showing that the complement of a large ball in H is included in $C_{n,X}$. For a further consequence of strong squeezing we consider a smooth N dimensional positively invariant surface. We assume that it is "blocked" in the sense that $\lambda(u) > \frac{\lambda_N+\lambda_{N+1}}{2}$ for $u \in \sum$ and $\lambda(u) = \lambda(P(u))$ with $P(u)$ the projector on the tangent space at u to $\sum$. We show that under these assumptions, as long as the distance from some solution $S(t)u_0$ to $\sum$ in attained on $\sum$, it must decay exponentially (at an explicit uniform rate).

We now proceed to describe the initial data for our construction. They form the smooth oriented boundary Γ of an bounded, open, connected set D included in $P_N H$. N is chosen sufficiently large such that $\lambda_{N+1} - \lambda_N > 0$ is a gap satisfying (4.14) and such that $\lambda_{N+1} > 5(\lambda_m + \lambda_{m+1})$ with a satisfying also (4.14). We denote at each net by $P(u)$ the projection on the space $N(u)R + T_n(\Gamma)$ where $T_u(\Gamma)$ is the tangent space at u to Γ; we design by $\nu(u)$ the outward unit normal to Γ and we set $\lambda(u) = \lambda(P(u)), \Lambda(u) = \Lambda(P(u))$. Then the properties of Γ are

$$\Lambda(u) < \frac{\lambda_N + \lambda_{N+1}}{2} \text{ for any } u\epsilon\Gamma \tag{I}$$

$$\lambda(u) > \frac{\lambda_N + \lambda_{N+1}}{2} \text{ for any } u\epsilon\Gamma \tag{II}$$

$$(N(u), \nu(u)) > 0 \text{ for any } u\epsilon\Gamma \tag{III}$$

$$\Gamma \subset C_{N,X} \tag{IV}$$

$$\text{For any } u \in \Gamma\ ,\ N(u)\mathbb{R} + T_u(\Gamma) \subset C \tag{V}$$

Properties (I) and (II) assert that the initial surface Γ is "blocked". Property (III) shows that $\frac{d}{dt}S(t,u_0)\Big|_{t=0}$, at any $u_0 \in \Gamma$ points toward the interior of D. In applications Γ is usually a simple explicit set: a large sphere for the Kuramoto-Sivashinski equation.

Ultimately, we use the spectral blocking, strong squeezing and volume decay properties in order to construct starting from Γ the inertial manifolds. We denote by $\sum$ the integral manifold having Γ as initial data:

$$\sum = \bigcup_{t>0} S(t)\Gamma \tag{4.17}$$

We establish first using (I) and the spectral blocking property the fact that projection P_N at any point of $\sum$ is a regular map (has invertible Jacobian). From the results in Theorem

4.4 and condition (IV) for Γ it follows that $\sum \subset C_{N,X}$. Since we may take Γ to lie far away from X; it follows that $\sum \cap X = \phi$ and thus, $P_N \sum \cap P_N X$ is void. We show that the closure of $P_N \sum$, $\overline{P_N \sum}$ is included in the union of the disjoint sets $P_N X \cup \Gamma \cup P_N \sum$. We use next the isoperimetric inequality and the exponential decay of surfaces of dimension larger or equal to $N-1$ to show that $\overline{P_N \sum} \supset D$. From the backward uniqueness theorem for solutions of an equation and (III) we deduce that for P in a neighborhood of Γ in D the fiber $P_N^{-1}\{p\} \cap \sum$ consists of a single point. Since P_N is regular at $\sum$ and since $P_N \sum$ is connected we deduce that P_N restricted to $\sum$ is injective. It follows that $D = P_N \sum \cup P_N X \cup \Gamma$ and we can define on D the inverse Φ of P_N, $\Phi : D \to E, \Phi\Big|_{\Gamma} = \{\text{identity}\}$. We show, using the strong squeezing property and (V) (Theorem 4.2) that

$$|(1 - P_N)(\Phi(r_1) - \Phi(r_2))| \leq \frac{1}{3}|P_N(\Phi(r_1) - \Phi(r_2)| \tag{4.18}$$

for any r_1, r_2 in D. Finally we show using (II) and the spectral blocking that for any u_0, $dist(S(t)u_0, \sum)$ decreases exponentially. We conclude that $\sum$ is an inertial manifold satisfying, beside properties (4.1), (4.2), (4.3), and (4.19) $\sum$ is the graph of an explicit Lipschitz map (4.20) $\sum$ is the closure of a smooth manifold (21) the N-dimensional volume of $\sum$ is finite.

This concludes the outline of the construction of the integral inertial manifold. Needless to say, it lends itself to fast and robust numerical algoritms. Full details may be found in [8].

V. CONCLUSION

A low dimensional vector field skeleton underpins "strong" chaos for the K-S models of turbulent interfaces. Heretofore it was unsuspected, because of the extreme numerical sensitivity of chaos in dissipative PDEs. Indeed, low precision methods of integration based on second order schemes [31] are adequate to compute tables of Lyapunov exponents; they wash out the subtle architecture mirrored by repeated bifurcations and intermittencies. High precision, high speed, parallel codes on future parallel architecture machines shall play a crucial role in definitely bridging the gap between strong dynamical chaos and fully developed turbulence. From a theoretical view point, the fact that a small, yet exotic zoo of hyperbolic points and Tori generates strong chaos supports the current analytic work initiated [6] by C. Foias, P. Constantin, R. Temam and B. Nichols. We presently aim at constructing optimal inertial normal forms for the dynamical vector fields on the inertial manifolds at different α-regimes. We suspect that the zoo of dynamically relevant strange fixed points will be enhanced by specimens with a Cantor-like structure in space (this has been proven by Michelson [45], for $\alpha = \infty$, for K-S). Hence, spatial chaos would intermingle with temporal chaos as the bifurcation parameter is increased to another order of magnitude.

ACKNOWLEDGMENTS

The author was supported by the US Department of Energy, Office of Scientific Computing under contract KC-07-01-01-0 and the US Department of Energy under contract W-7405-ENG-36. Different parts of this survey article focus on joint research with P. Constantine, C. Foias, J. M. Hyman and R. Temam. We acknowledge international travel support from NATO under contract № 85/0520j.

REFERENCES

1. P. Clavin, "Dynamical Behavior of Premixed Flame Fronts in Laminar and Turbulent Flows," Prog. Energy. Combust. Sci. 11 (1985), 1-59.
2. P. Constantine and C. Foias, Comm. Pure Appl. Math. 38 (1985), 1-27.
3. P. Constantine, C. Foias and R. Temam, Memoirs AMS 53 (1985) 314, vii+.67 pp.
4. P. Constantine, C. Foias, O. P. Manley and R. Temam, C. R. Acad. Sci. Paris I, 297 (1983), 599-602.
5. P. Constantine, C. Foias, O. P. Manley and R. Temam, J. Fluid Mech. 150 (1985) 427-440.
6. P. Constantine, C. Foias, B. Nicolaenko and R. Temam, "Integral Manifolds and Inertial Manifolds for Dissipative PDEs (submitted).
7. J. D. Farmer, E. Jen, A. Brandstäter, J. Swift, H. L. Swinney, A. Wolff and J. P. Crutchfield, "Low Dimensional Chaos in a Hydrodynamic System," Phys. Rev. Lett. 51, 16 (1983) 1442-1445. See also J. P. Gollub and H. L. Swinney, Phys. Rev. Lett. 35 (1975) 927.
8. C. Foias, B. Nicolaenko and R. Temam, "Asymptotic Study of an Equation of G. I. Sivashinsky for Two Dimensional Turbulence of the Kolmogorov Flow," to appear, Proc. Paris Acad. Sci.
9. C. Foias and R. Temam, C. R. Acad. Sci. Paris, I, 295 (1982) 239-241.
10. C. Foias and R. Temam, C. R. Acad. Sci. Paris, I, 295 (1982) 523-525.
11. C. Foias and R. Temam, Mathematics of Computation 43 (1984), 117-133.
12. C. Foias, G. R. Sell and R. Temam, C. R. Acad. Sci. Paris, I, 301 (1985) 139-141.
13. C. Foias, G. R. Sell and R. Temam, "Inertial Manifolds for Dissipative PDEs (submitted).
14. C. Foias, B. Nicolaenko, G. R. Sell and R. Temam, C. R. Acad. Sci. Paris, I, 301 (1985) 285-288.
15. C. Foias, B. Nicolaenko, G. R. Sell and R. Temam, "Inertial Manifolds and an Estimate of Their Dimension for the Kuramoto-Sivashinsky Equation (submitted).
16. P. L. Garcia-Ybarra and M. G. Velarde, "Oscillatory Marangoni-Benard Interfacial Instability and Capillary-Gravity Waves in Single and Two-Component Liquid Layers with or without Soret Thermal Diffusion," to appear.

17. P. L. Garcia-Ybarra, J. L. Castillo and M. G. Velarde, "Benard-Marangoni Convection with a Deformable Interface and Poorly Conducting Boundaries," to appear.
18. M. Golubitsky and D. G. Schaeffer, "Singularities and Groups in Bifurcation Theory," Springer-Verlag, New York (1985).
19. C. Grebogi, E. Ott and Y. A. Yorke, "Crisis, Sudden Changes in Chaotic Attractors and Transient Chaos," Physica 7D (1983) 181-200.
20. C. Grebogi, E. Ott and Y. A. Yorke, "Fractal Basin Boundaries, Long-Lived Chaotic Transients and Unstable-Unstable Pair Bifurcation," Phys. Rev. Lett. 50, 13 (1983) 935-938.
21. C. Grebogi, S. W. McDonald, E. Ott and Y. A. Yorke, "Final State Sensitivity: An Obstruction to Predictability," Phys. Lett. 99A, 9 (1983) 415-418.
22. C. Grebogi, S. W. McDonald, E. Ott and Y. A. Yorke, "Structure and Crises of Fractal Basin Boundaries," Phys. Lett. 107A, 2 (1985) 51-54.
23. C. Grebogi, E. Ott and Y. A. Yorke, "Super Persistent Chaotic Transients," Ergod. Th. and Dynam. Sys. 5 (1985) 341-372.
24. C. Grebogi, S. W. McDonald, E. Ott and Y. A. Yorke, "Fractal Basin Boundaries," Physica 17D (1985) 125-153.
25. J. Guckenheimer and P. H. Holmes, "Nonlinear Oscillations, Dynamical Systems and Bifurcation of Vector Fields," Springer-Verlag (1985).
26. J. Guckenheimer, "Strange Attractors in Fluids: Another View," Annual Review of Fluid Mechanics (1986).
27. J. Guckenheimer, private communication.
28. J. M. Hyman and B. Nicolaenko, "The Kuramoto-Sivashinsky Equation: a Bridge Between PDEs and Dynamical Systems," Physica 18D (1986), 113-126.
29. J. M. Hyman, "Numerical Methods for Nonlinear Differential Equations," Nonlinear Problems: Present and Future, A. R. Bishop, D. K. Campbell and B. Nicolaenko, Eds., North-Holland Publ. Co., (1982) 91-107.
30. J. M. Hyman and M. Naughton, "Adaptive Static Rezoning Methods," Lectures in Applied Math. 22, Part I (1985) 321-343.
31. P. Manneville, "Liapunov Exponents for the Kuramoto-Sivashinsky Model," Proc. Conf. on Macroscopic Modeling of Turbulent Flows, U. Frisch, Ed., Springer-Verlag, Lecture Notes in Physics 230 (1985), 319-326.
32. B. Nicolaenko and S. Zaleski, "Crisis of Chaos for Models of Interface Turbulence," to appear in Physica D.
33. B. Nicolaenko and B. Scheurer, "Remarks on the Kuramoto-Sivashinsky Equation," Physica 12D (1984) 331-395.

34. B. Nicolaenko, B. Scheurer, and R. Temam, "Quelques proprietes des attracteurs pourl'equation de Kuramoto-Sivashinsky," C. R. Acad. Sci. Paris 298 (1984) 23-25.
35. B. Nicolaenko, B. Scheurer, and R. Temam, "Attractors for the Kuramoto-Sivashinsky Equations," Physica 16D (1985) 155-183.
36. B. Nicolaenko, B. Scheurer, and R. Temam, "Attractors for the Kuramoto-Sivashinsky Equations," AMS-SIAM Lectures in Applied Mathematics 23, 2 (1986) 149-170.
37. B. Nicolaenko, B. Scheurer, and R. Temam, "Attractors for Classes of Nonlinear Evolution of Partial Differential Equations," in preparation.
38. G. I. Sivashinsky and A. Novick-Cohen, "Interfacial Instabilities in Dilute Binary Mixtures Change of Phase, to appear in Physica D.
39. Z. S. She, U. Frisch and O. Thual, "Homogenization and Visco-Elasticity of Turbulence," Proc. Conf. on Macroscopic Modeling of Turbulent Flows, U. Frisch, Ed., Springer-Verlag Lecture Notes in Physics 230 (1985) 1-13.
40. K. Shreenivasan, "Transition and Turbulence in Fluid Flows and Low-Dimensional Chaos," Frontiers in Fluid Mechanics, S. H. Davis and J. L. Lumley, Eds., Springer-Verlag (1985) 41-67.
41. R. Temam, "Navier Stokes Equations and Nonlinear Functional Analysis," SIAM, Philadelphia, 1983.
42. R. Temam, "Infinite Dimensional Dynamical Systems of Fluid Mechanics," AMS-Summer Res. Institute "Nonlinear Funct. Anal. Appl." (Berkeley, 1983).
43. M. G. Velarde and C. Normand, Sci. Amer. 243 (1980) 92.
44. M. G. Velarde and J. L. Castillo, "Convective Transport and Instability Phenomena, J. Zierep and H. Oertel, Jr., Eds., Braun-Verlag, Karlsruhe (1982).
45. D. M. Michelson, "Steady-States for the Kuramoto-Sivashinsky Equation," preprint.

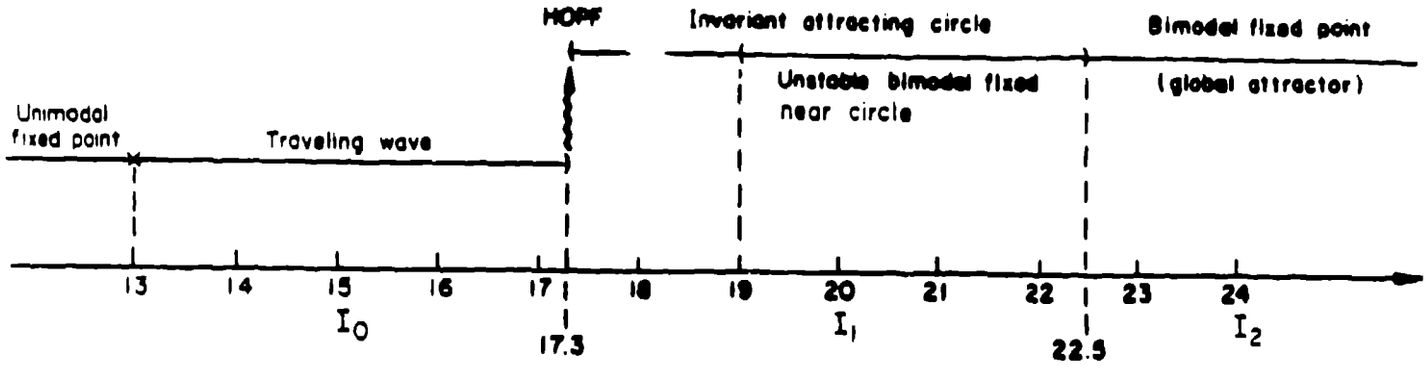

Fig. 1. The stable solution manifolds have a simple structure when α is small.

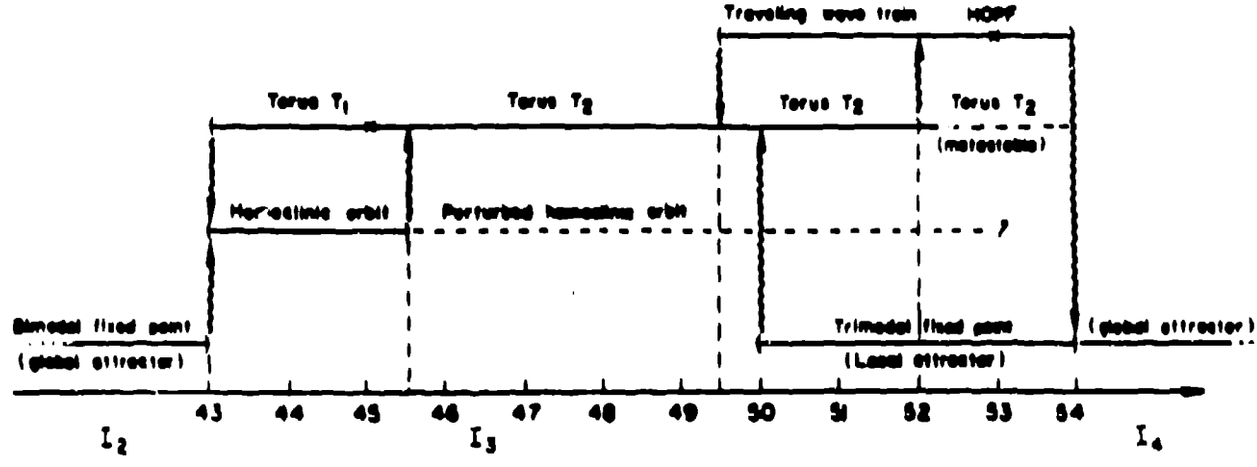

Fig. 2. As the bifurcation parameter increases, complex homoclinic and quasiperiodic behavior sets in (number of unstable modes between 3.2 and 3.6).

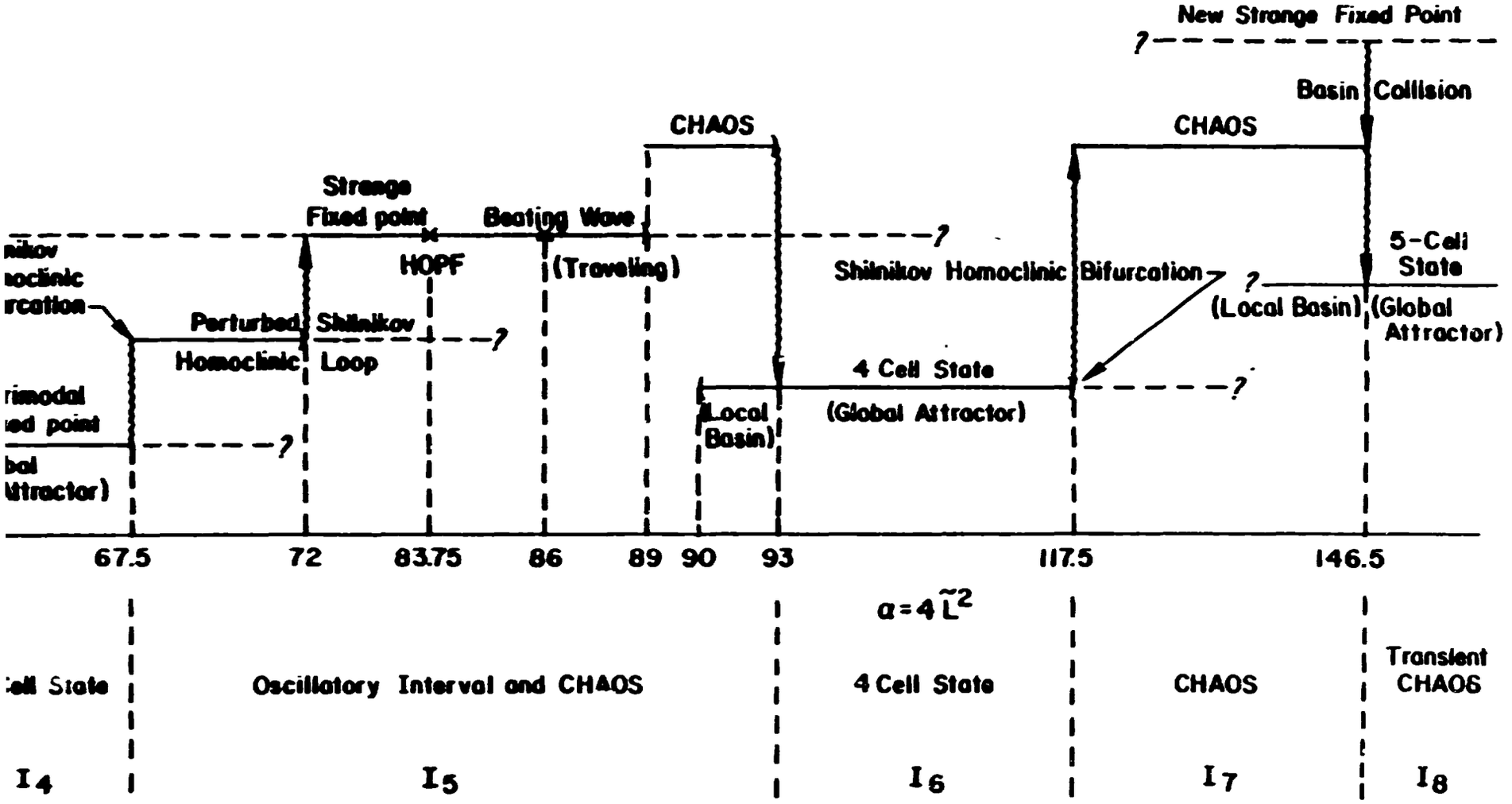

Fig. 3. A low-dimensional vector field skeleton underlies these weakly chaotic regimes (number of unstable modes between 3.6 and 6).

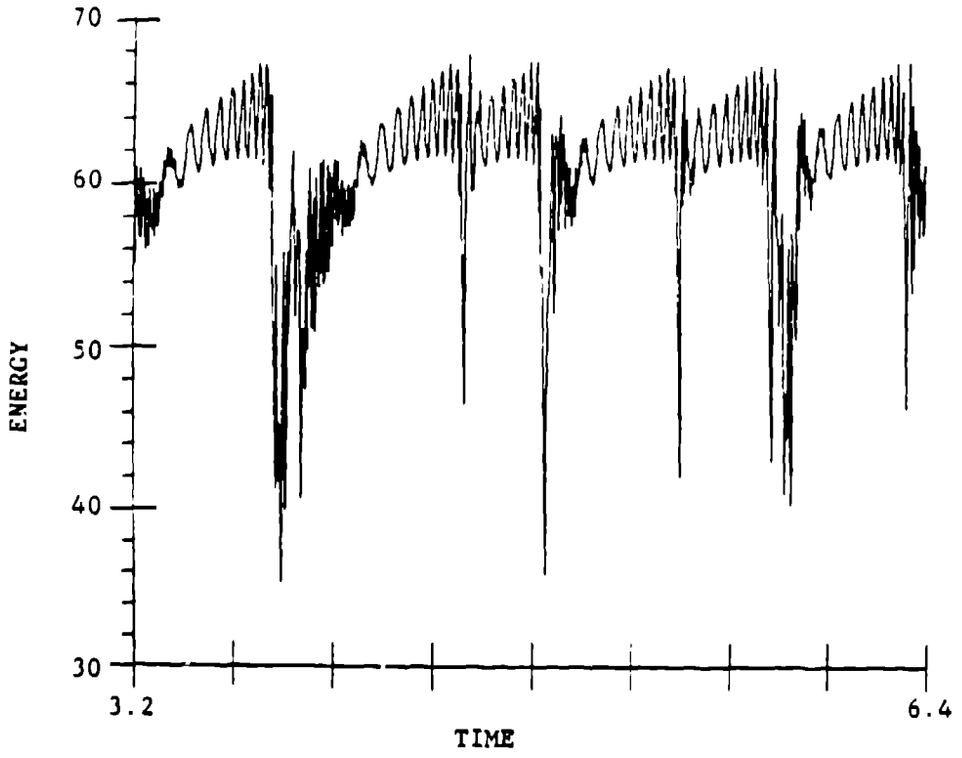

Fig. 4. The energy has near periodic bursts on the Shilnikov homoclinic loop and then spirals around the hyperbolic point (α = 67.5).

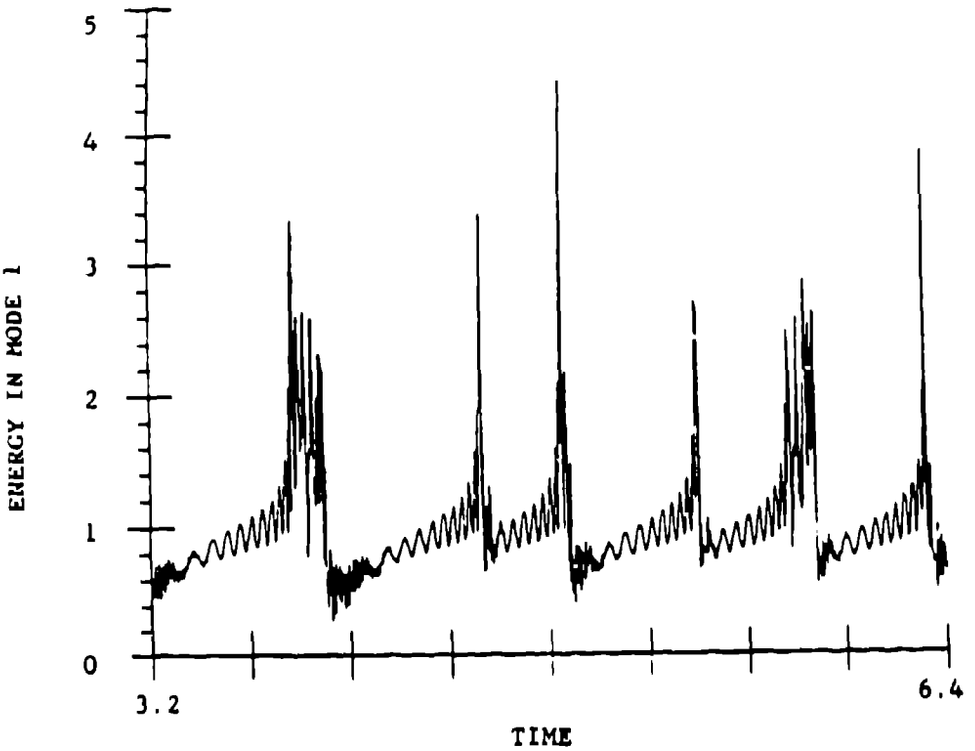

Fig. 5. The energy in the first mode is low during the small oscillations near the trimodal cellular hyperbolic point (α = 67.5).

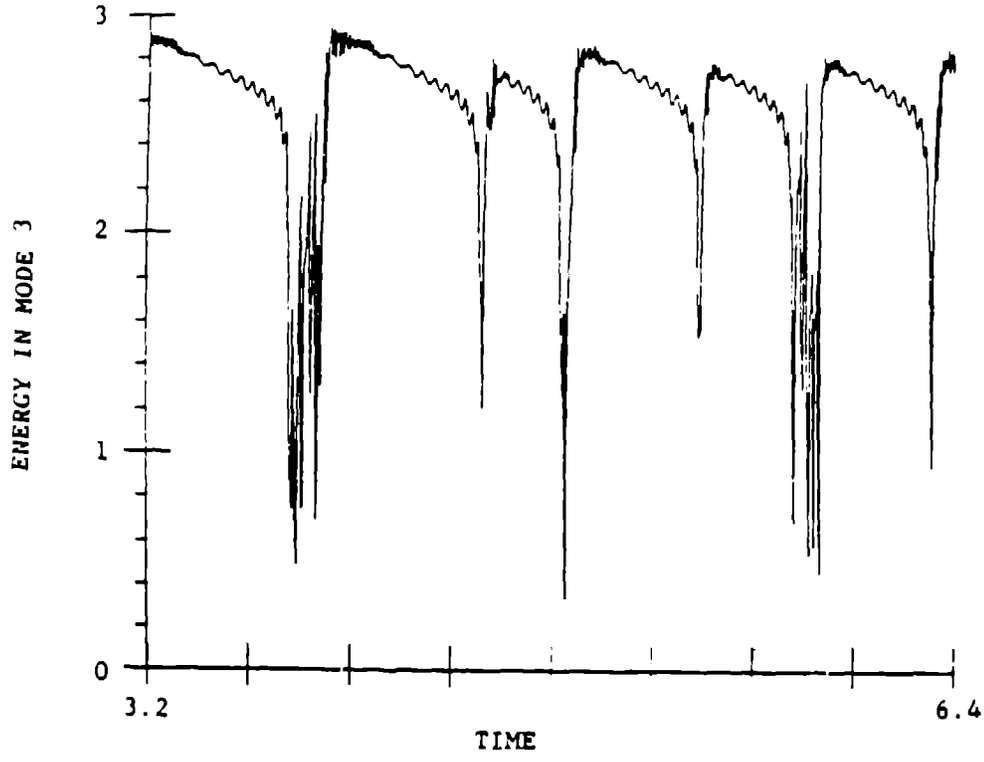

Fig. 6. The energy in the third mode is high in the neighborhood of the spiral hyperbolic point, whose components are only harmonics of three (α = 67.5).

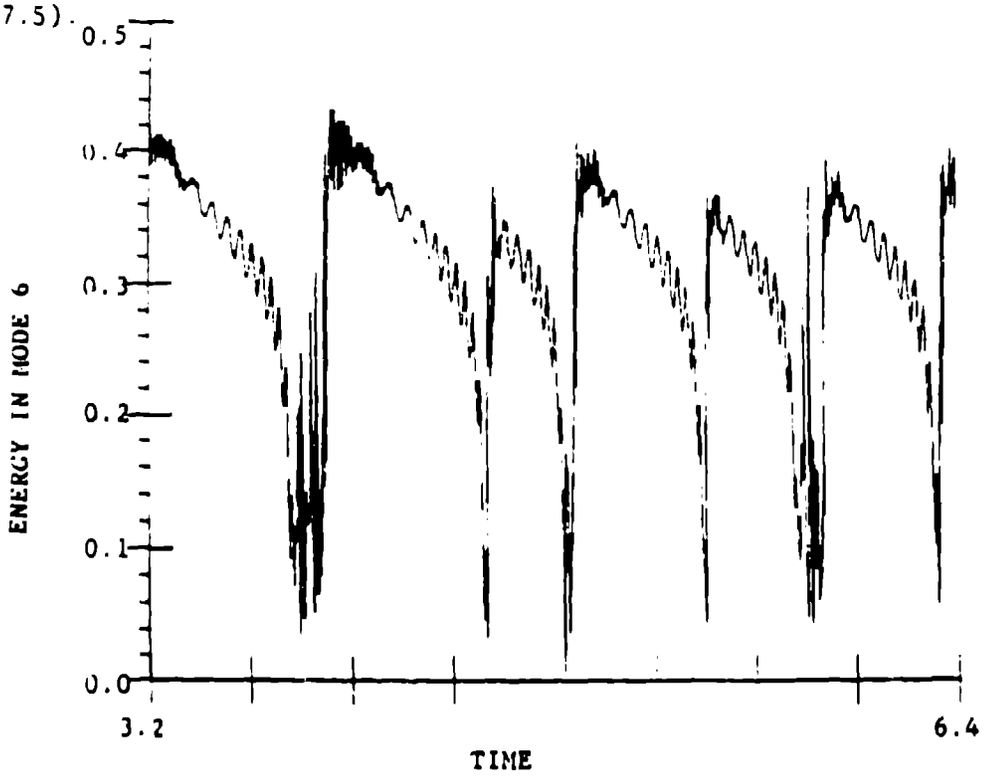

Fig. 7. The energy in the sixth mode is substantial next to $\tilde{u}_3$; high frequency oscillations are clearly distinguished close to this cellular point (α = 67.5).

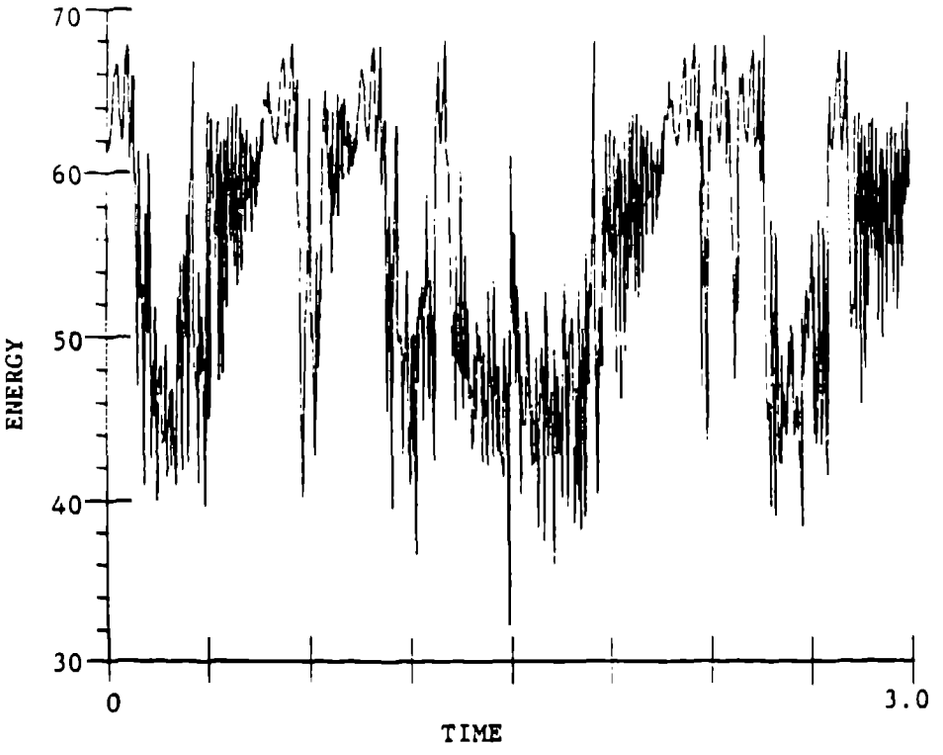

Fig. 8. For the perturbed Shilnikov loops, the orbit goes into chaotic puffs array from the trimodal point (α = 68).

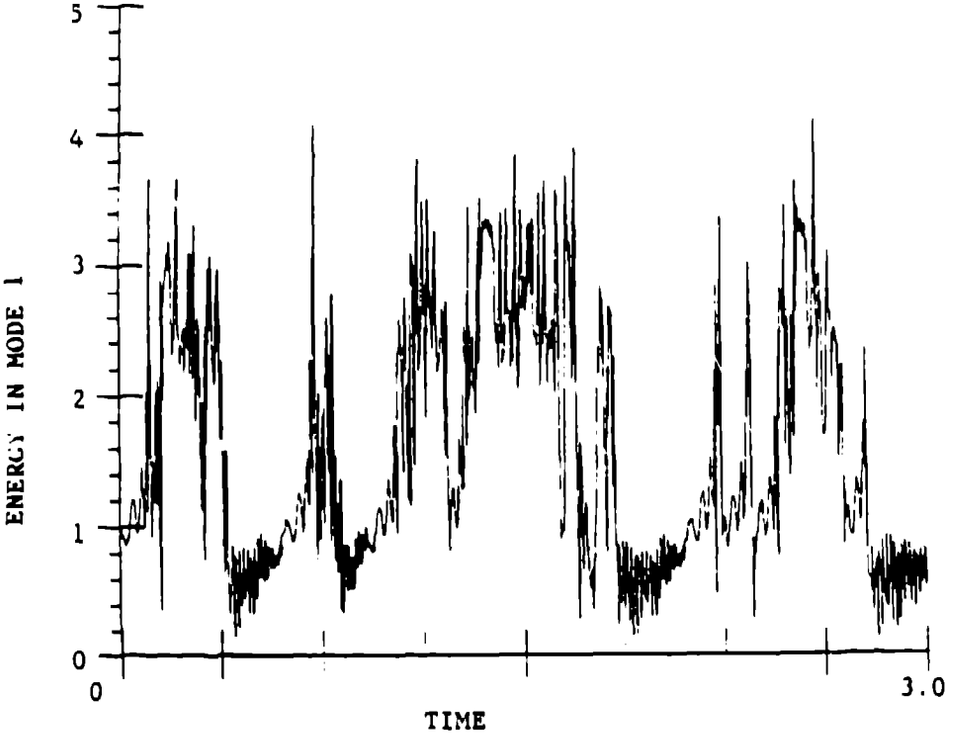

Fig. 9. The energy in the first mode is high clearing the chaotic excursions; their duration is comparable to the stagnation time near u_3 (α = 68).

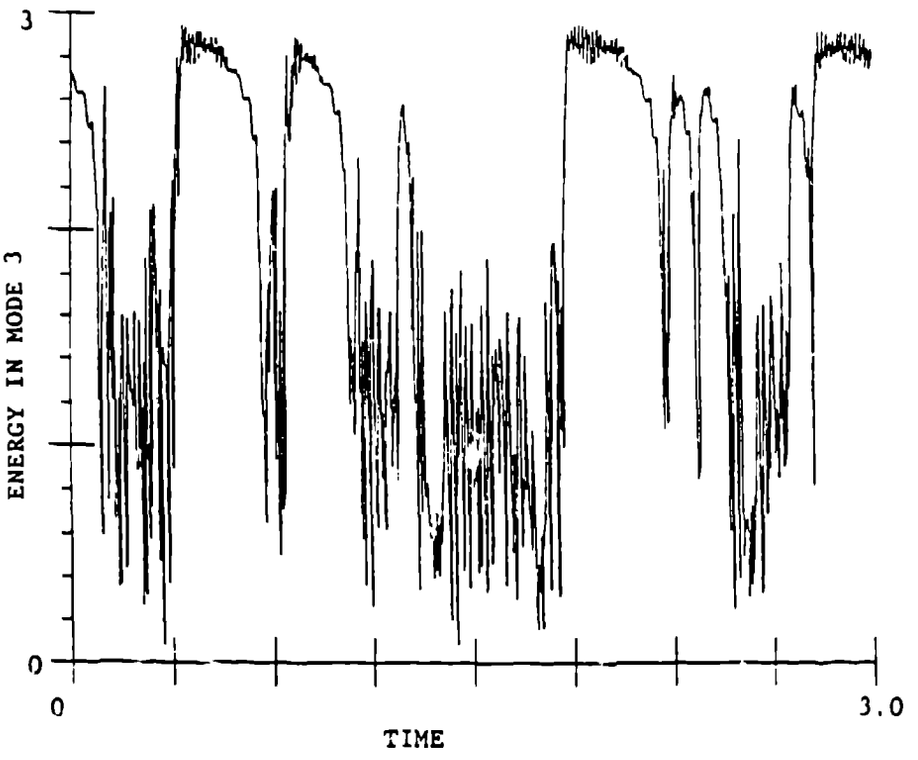

Fig. 10. The energy in Mode 3 clearly shows the homoclinic tangle between the stable and unstable manifolds of $\tilde{u}_3$ (α = 68).

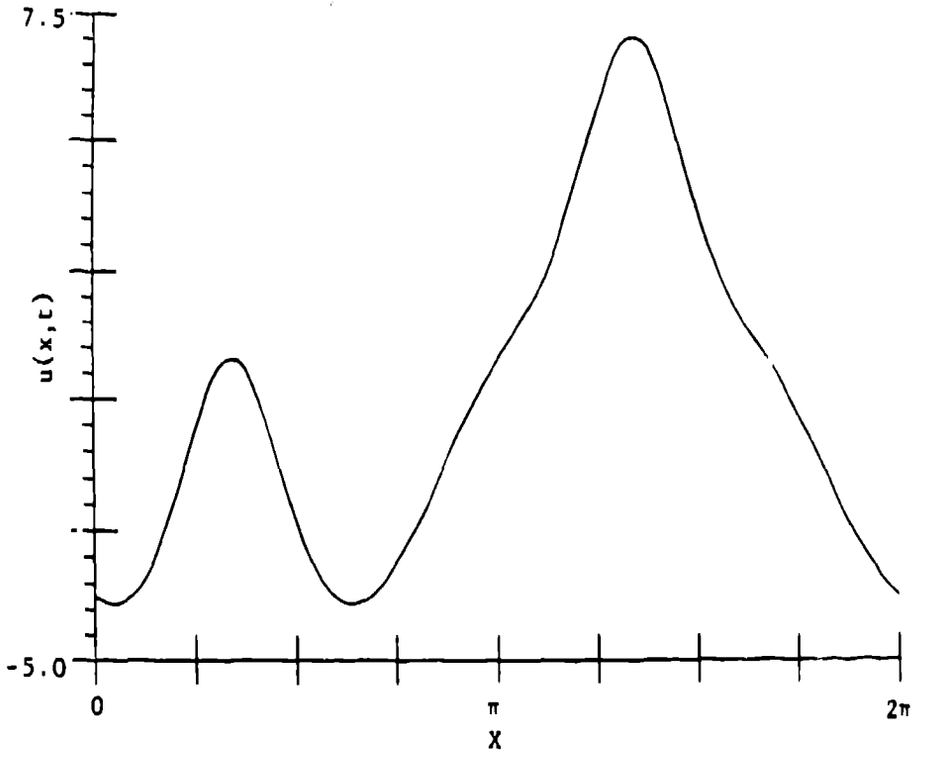

Fig. 11. This strange fixed point becomes a global attractor at α = 72. It has energy in all first seven Fourier Modes (α = 72).

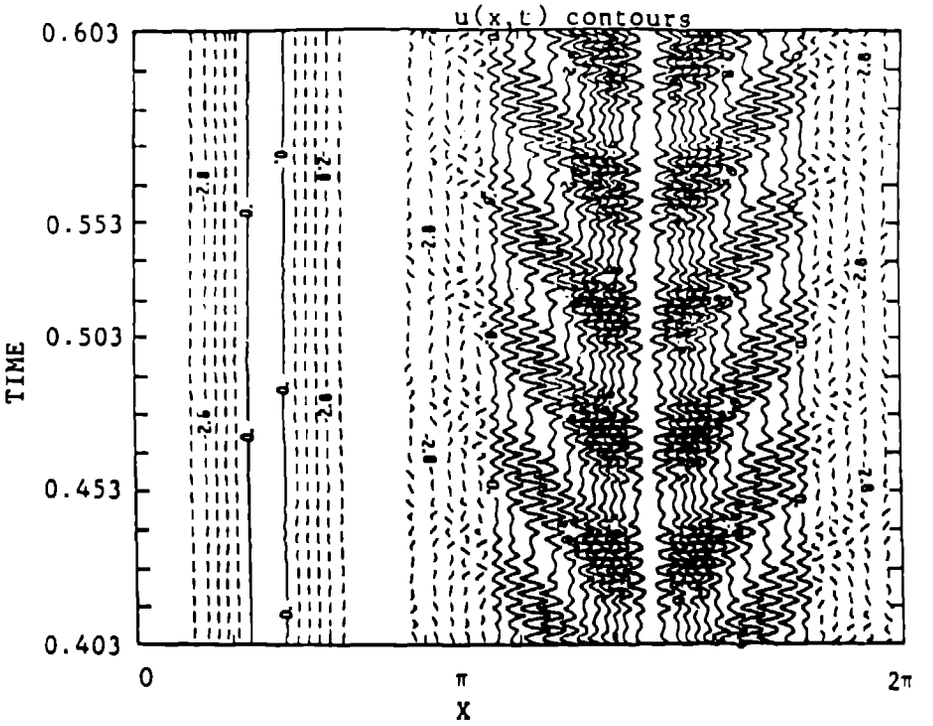

Fig. 12. The strange fixed point undergoes Hopf bifurcation. The oscillations are localized on the tip of the higher hump (α = 84.25).

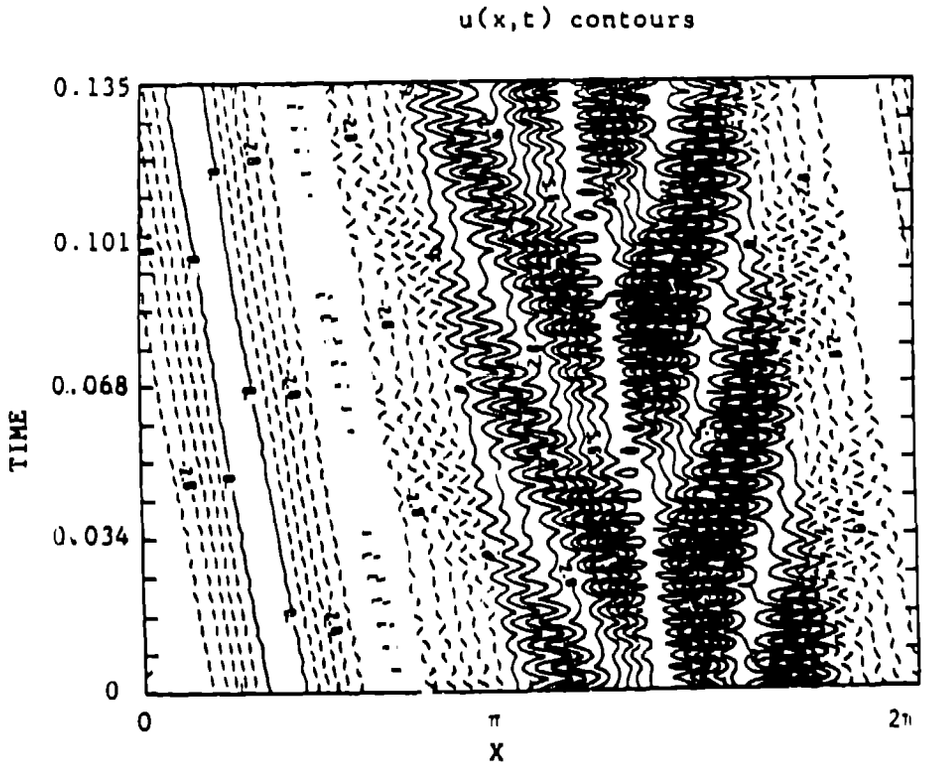

Fig. 13. The strange fixed point has further gone into a traveling beating wave. The beating is still localized on the higher hump (α = 87).

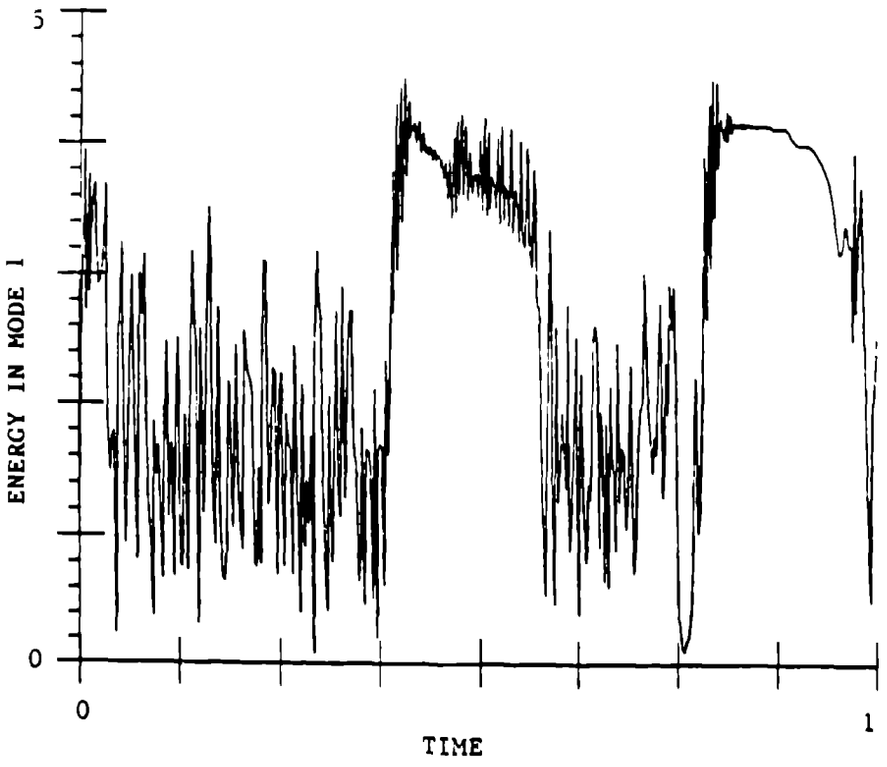

Fig. 14. Crisis of chaos looms. Intermittencies are observed, with small amplitude, high frequency oscillations (α = 91).

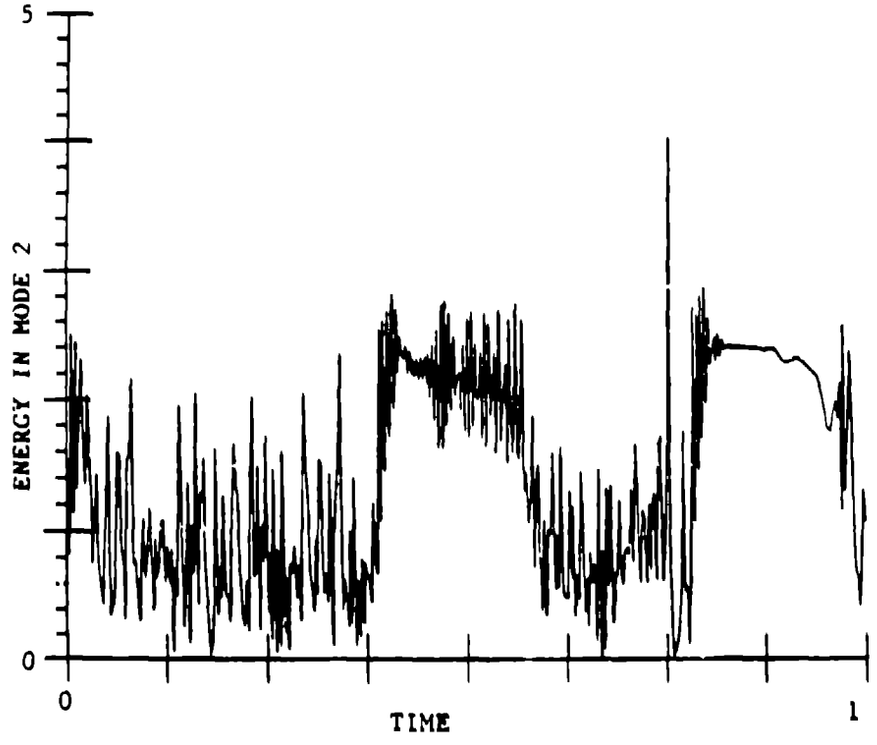

Fig. 15. Within the intermittent windows, energy in Modes 2 and 1 are comparable. They betray the strange, two-humped fixed point (α = 91).

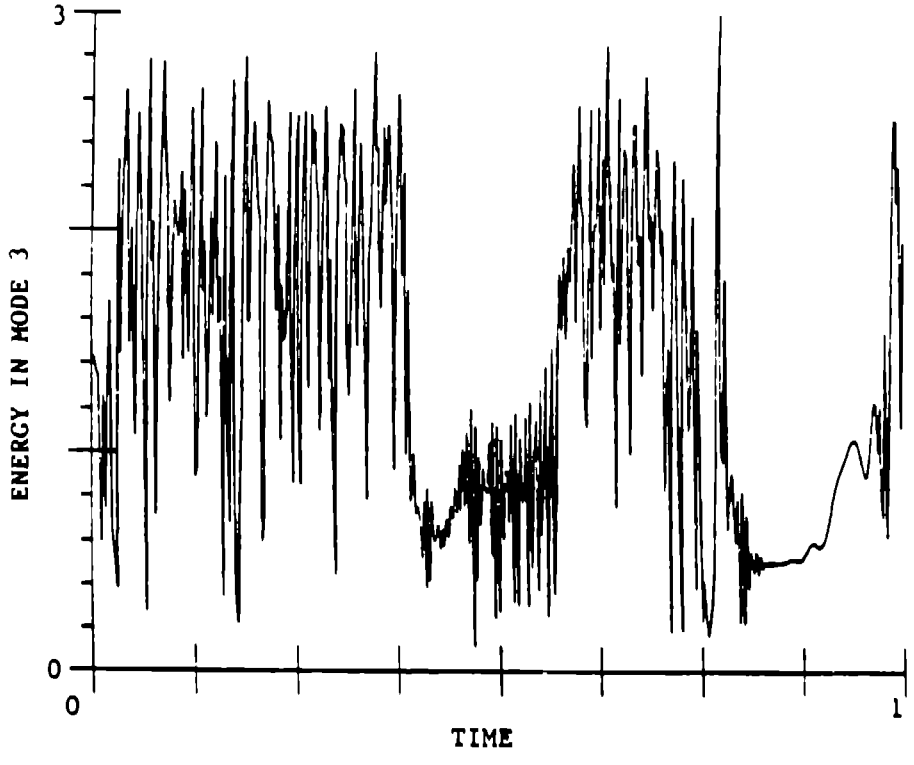

Fig. 16. Energy in Mode 3 is small when the orbit wanders close to the stable manifold of the strange hyperbolic point ($\alpha = 91$).

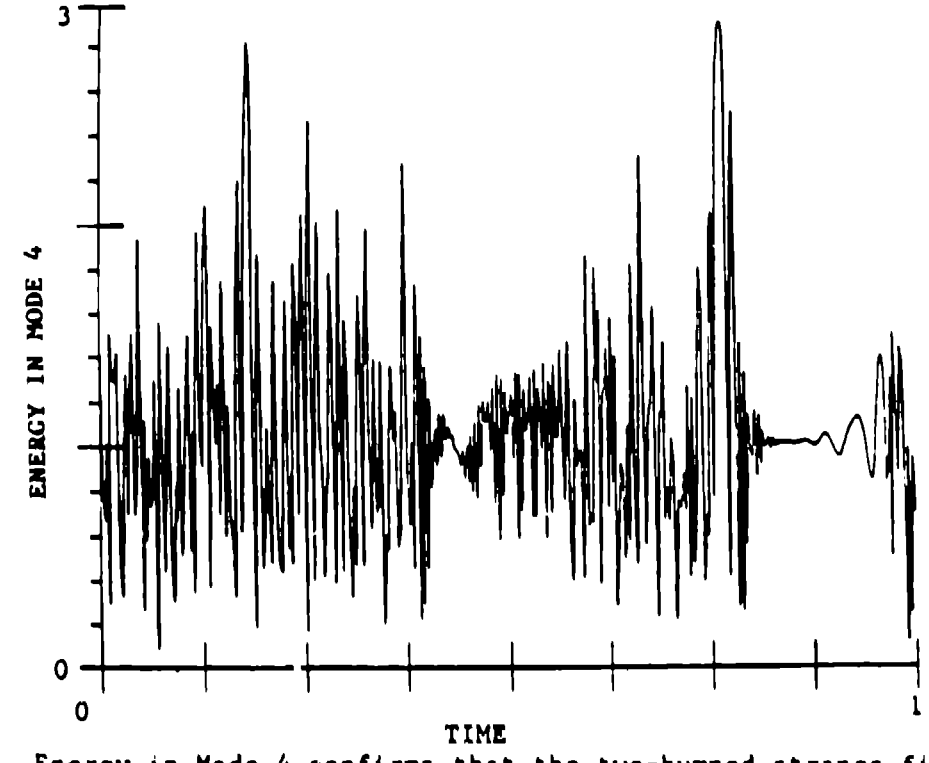

Fig. 17. Energy in Mode 4 confirms that the two-humped strange fixed point sits on the boundary between the basins of resp. the chaotic attractor and the quadrimodal state $\tilde{u}_4$ ($\alpha = 91$).

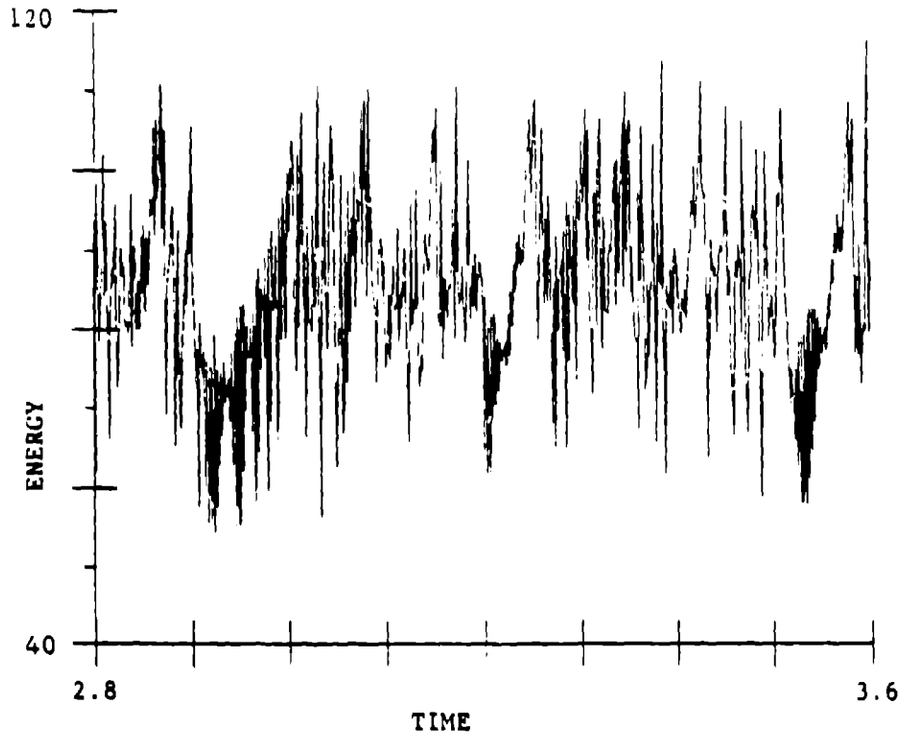

Fig. 18. The energy undergoes high frequency oscillations close to the quadrimodal cellular state, before going into chaotic excursions (α = 117.5).

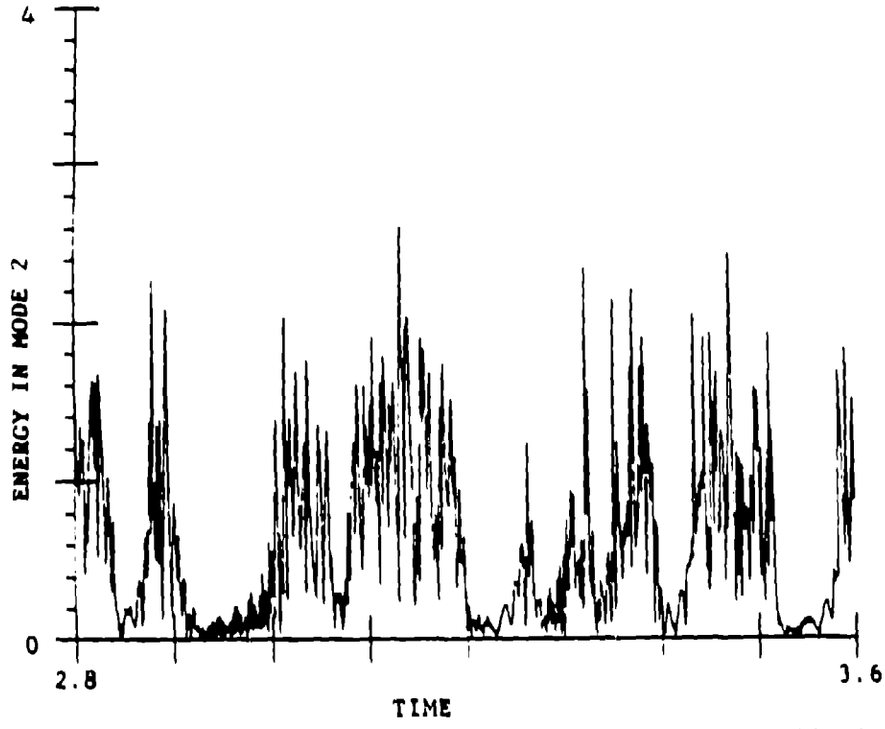

Fig. 19. The energy in Mode 2 is very small in the neighborhood of $\tilde{u}_4$ (α = 117.5).

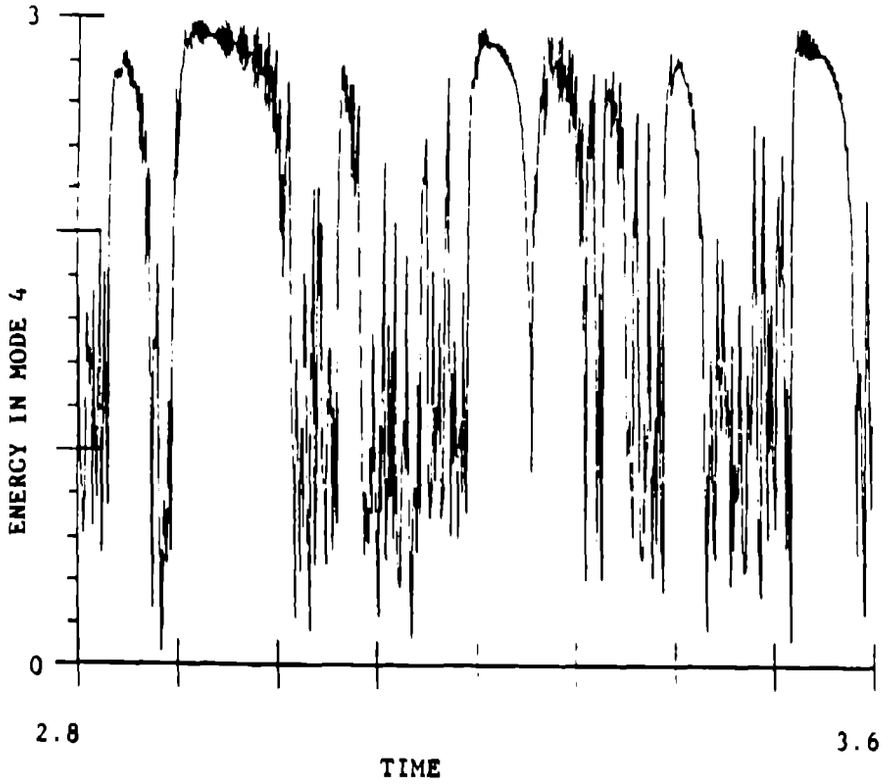

Fig. 20. The energy in Mode 4 clearly shows the trajectory spiraling around the cellular state, before bursting into homoclinic tangles (α = 117.5).

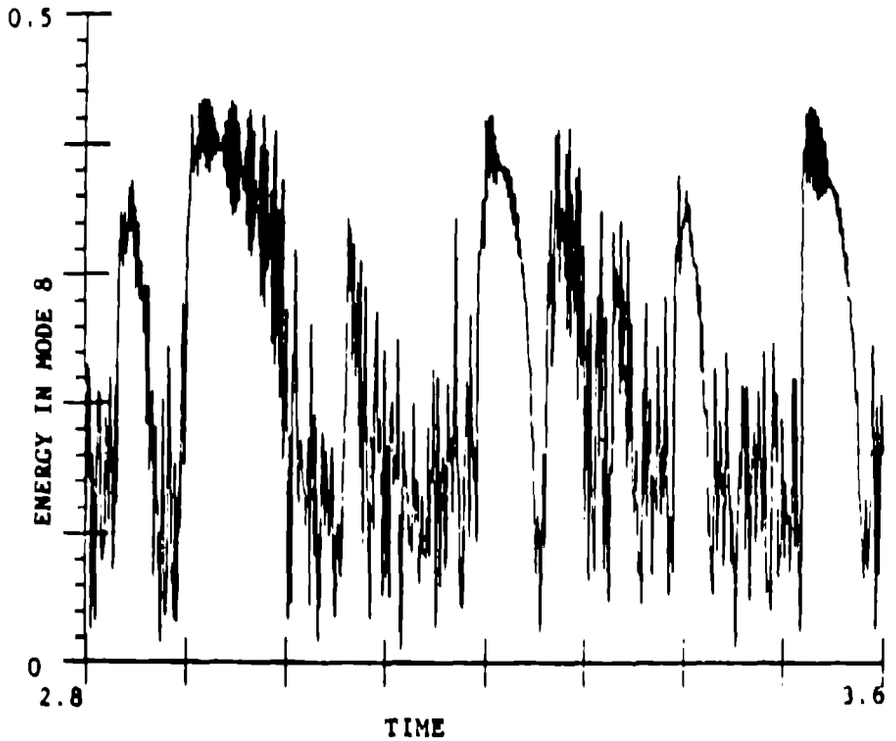

Fig. 21. The energy in Mode 8 confirms the picture of a perturbed Shilnikov loop around $\tilde{u}_4$, as a mechanism for onset of chaos (α = 117.5).